Regional and seasonal stratospheric temperature trends in the last decade (2002–2014) from AMSU observations

Beatriz M. Funatsu, Chantal Claud, Philippe Keckhut, Alain Hauchecorne, Thierry Leblanc

AGU PUBLICATIONS

JGR

Journal of Geophysical Research: Atmospheres

RESEARCH ARTICLE
10.1002/2015JD024305

Key Points:
- Stratosphere cooled at a global mean rate of -0.2 ± 0.3 to -0.5 ± 0.4 K/decade in the 2002–2014 period
- Trends range from -0.5 ± 0.3 to -0.7 ± 0.3 K/decade above 30 km in the tropics
- Regional trends by AMSU (2002–2014) and lidars (greater than two decades) confirm continuous stratospheric cooling

Correspondence to:
B. M. Funatsu,
bmf.amit@gmail.com

Citation:
Funatsu, B. M., C. Claud, P. Keckhut, A. Hauchecorne, and T. Leblanc (2016), Regional and seasonal stratospheric temperature trends in the last decade (2002–2014) from AMSU observations, *J. Geophys. Res. Atmos.*, *121*, 8172–8185, doi:10.1002/2015JD024305.

Received 2 OCT 2015
Accepted 27 JUN 2016
Accepted article online 4 JUL 2016
Published online 19 JUL 2016

Regional and seasonal stratospheric temperature trends in the last decade (2002–2014) from AMSU observations

Beatriz M. Funatsu[1], Chantal Claud[2], Philippe Keckhut[3], Alain Hauchecorne[3], and Thierry Leblanc[4]

[1]CNRS, LETG-Rennes-COSTEL UMR 6554, Université Rennes 2, Rennes, France, [2]LMD, CNRS UMR 5839, IPSL, École Polytechnique, Palaiseau, France, [3]LATMOS, CNRS UMR 8190, IPSL, Université de Versailles Saint-Quentin, Guyancourt, France, [4]Jet Propulsion Laboratory, California Institute of Technology, Wrightwood, California, USA

Abstract Stratospheric temperature trends for the period 2002–2014 have been estimated using NOAA's Integrated Microwave Inter-calibration Approach (IMICA) version of advanced microwave sounding unit (AMSU) on AQUA satellite. In this period the stratosphere continued cooling over most of the globe with a rate ranging from −0.4 ± 0.3 to −0.5 ± 0.4 K/decade above 25 km. Considering specific latitude bands, trends are highly variable with height. In the tropical region, trends vary from −0.5 ± 0.3 K/decade for channel 12 (~30 km) to −0.7 ± 0.3 K/decade for higher channels and present small seasonal variability in the intensity of cooling. In the polar regions and in the midlatitudes, trends for all channels are negative but not significant; uncertainties are large due to the high dynamical variability particularly in high latitudes. There is also large seasonal variability, with southern midlatitudes seasonal trends significant during summer (December, January, February) and autumn (March, April, May) above ~25 km, with values ranging from −1.0 ± 0.5 to −0.6 ± 0.5 K/decade. Regional trends estimated with AMSU and long-term lidar measurements (over two decades) confirm stratospheric cooling in the northern midlatitudes and tropical regions. The effect of the length of the short series on trends was found to be small outside polar regions. It was found to be large in polar regions with about 1 K changes in trend depending on start dates of the time series.

1. Introduction

Stratospheric temperature trends are fingerprints of climate change, reacting to radiative, chemical, and dynamical forcing. A large range of observations and climate model simulations for the period until ~2005 indicate that the stratosphere cooled in most of the layer up to 50 km in altitude due to both the decrease in stratospheric ozone concentration and the increase in tropospheric greenhouse gases (GHG) [*Hansen et al.*, 1997; *Waugh et al.*, 1999; *Shine et al.*, 2003; *Cagnazzo et al.*, 2006; *Austin et al.*, 2009; *Son et al.*, 2009; *Hu and Fu*, 2009; *Randel et al.*, 2009; *Keckhut et al.*, 2011; *Gillet et al.*, 2012; *Angot et al.*, 2012; *Garfinkel et al.*, 2013a; *Young et al.*, 2013; *Aquila et al.*, 2016], with a mean cooling of 0.5–1.5 K/decade over much of the globe for the period 1979–2007 [*Randel et al.*, 2009]. *Aquila et al.* [2016] used the NASA Goddard Earth Observing System Chemistry-Climate Model (GEOSCCM) and assessed the contributions of GHG, ozone depleting substances (ODS), volcanic eruptions, and the solar cycle in global scale, for the period of 1979–2014, and found that in the period before 2000 the cooling was dominated by ODS. After 2000, their simulations showed that trends have been dominated by GHG effects (also with important contribution by the ascending phase of the solar cycle), and cooling values were estimated to have weakened substantially within the whole stratospheric column. In effect, since the implementation of the Montreal Protocol in the late 1980s, the levels of ODS have decreased in the stratosphere and ozone concentrations have started to climb [*World Meteorological Organization*, 2014]. These changes in the chemical composition impact the radiative balance in the stratosphere, potentially leading to a reversal of cooling trends in the stratosphere. Could substantial changes in trends be already observed?

Temperature measurements in the stratosphere are limited to few sources with only spaceborne instruments providing temporally continuous global coverage temperature measurements since the late 1970s, first with the Stratospheric Sounding Unit (SSU) until early 2006 and with the Advanced Microwave Sounding Unit (AMSU) since 1998. SSU operated on NOAA platforms from 1979 to 2006, i.e., covering more than 25 years. It provided invaluable global-scale stratospheric temperature data; however, SSU data require special

processing before it can be used in climate applications [e.g., *Ramaswamy et al.*, 2001; *Keckhut et al.*, 2011; *Wang et al.*, 2012; *Nash and Saunders*, 2015]. Until recently, only one SSU-based temperature series were available for the climate community, but in the past few years new versions that addressed several issues of the former data set have been released [*Wang et al.*, 2012; *Zou et al.*, 2014; *Nash and Saunders*, 2015]. The first new release from NOAA in 2012 [*Wang et al.*, 2012] showed that the reprocessed SSU data trends seemed to become positive in the lower stratosphere (15–20 km); however, in the middle and upper stratosphere (above 25 km) the trend was not clear [*Thompson et al.*, 2012]. Analysis of version 2 of this data set [*Zou et al.*, 2014] has confirmed long-term cooling trends [*McLandress et al.*, 2015] in association with increasing CO_2, from ozone depletion caused by ODS, and the effects of the solar cycle (which was in the descending phase until the middle-to-late 2000s). Finally, a new version from the UK Met Office has been made available in 2015 [*Nash and Saunders*, 2015], which confirms cooling in the stratospheric column up to ~50 km.

After the retirement of the SSU instrument in 2005, AMSU has become the sentinel instrument for stratospheric temperature monitoring. AMSU has very different weighting functions than those of SSU, with better vertical resolution. The "stitching" of measurements of these two instruments is challenging due to their very different weighting functions. *McLandress et al.* [2015] have recently addressed this issue by merging nadir-sounding measurements from SSU and AMSU, with support of Michelson Interferometer for Passive Atmospheric Sounding data. They constructed global mean temperature data for SSU channels for the period 1979 to 2011 and found that the upper stratosphere (35–45 km) has cooled with a rate of $\sim -0.6 \pm 0.3$ K/decade from 2004 to 2012. This value is less negative than estimates for the preceding period (around −1 K/decade for the period 1979–2005), but they concluded that the differences found were not statistically significant. *Randel et al.* [2016] used SSU combined with data from the Aura Microwave Limb Sounder (MLS) and Sounding of the Atmosphere using Broadband Emission Radiometry (SABER) to form a data record spanning the period of 1979–2015 to study stratospheric multidecadal temperature trends, solar cycle variations, and volcanic effects. They found that over the more than three decades coverage period the stratosphere cooled with a rate of −0.1 to −0.2 K/decade at the lower stratosphere to ~−0.5 to −0.6 K/decade in the middle and upper stratosphere, but the cooling slowed down in the period of 1998–2015 compared to the earlier one (1979–1997).

Although *McLandress et al.* [2015] detected a global cooling of the stratosphere, the latitudinal, seasonal, and regional trends were not investigated, as done by *Randel et al.* [2016] from combined satellite observations. Here we examine these aspects using solely AMSU data, which has a finer vertical resolution compared to the SSU data. The ozone recovery is inhomogeneous across the latitudes [*Pawson et al.*, 2014]; thus, we do not know whether this is apparent in the trends. Also, the global-scale (Brewer-Dobson) and regional (stratospheric polar vortex and tropospheric blocking patterns) circulations may affect trends locally. Finally, there is also seasonal and interannual variability, for example, the occurrence and intensity of stratospheric sudden warming (SSW) events. We address these issues by examining recent stratospheric temperature trends using AMSU data for (a) separate latitude bands and (b) separate seasons, from the low to the middle stratosphere (up to around 45 km).

2. Data and Methods

2.1. AMSU

AMSU is a cross-scanning microwave-based sounder operating onboard NOAA, AQUA, and MetOp polar-orbiting platforms since late 1998 on NOAA 15. AMSU is composed of two modules of which the module -A was designed to give optimal information on the temperature profile from the surface up to around 50 km in altitude. Channels 9–14 sample at or above the tropopause region, with weighting functions peaking at approximately 18, 20, 25, 30, 35, and 40 km, respectively (Figure 1a). The horizontal resolution at the near-nadir field of view is approximately 48 km, and the vertical half width of the weighting functions is about 10 km.

Figure 1b shows the equatorial crossing local time of the current platforms that carry AMSU. NOAA and MetOp orbital hour data were obtained through the site http://www.ospo.noaa.gov/Products/ppp/navpage.html. Orbital data for NOAA 17 were not available after 2012; AQUA orbital data were taken from http://aqua.nasa.gov/content/about-aqua. NOAA platforms present a strong drift with time, while MetOp and AQUA satellites are maintained in near-fixed orbits. AMSU measurements in distinct platforms may present different values for the same target even for measurements taken at around the same time due to calibration issues. The NOAA Center for Satellite Applications and Research (STAR) has recently released intercalibrated brightness temperatures from the Advanced Microwave Sounding Unit-A (AMSU-A) sensors onboard NOAA 15, 16, 17, 18,

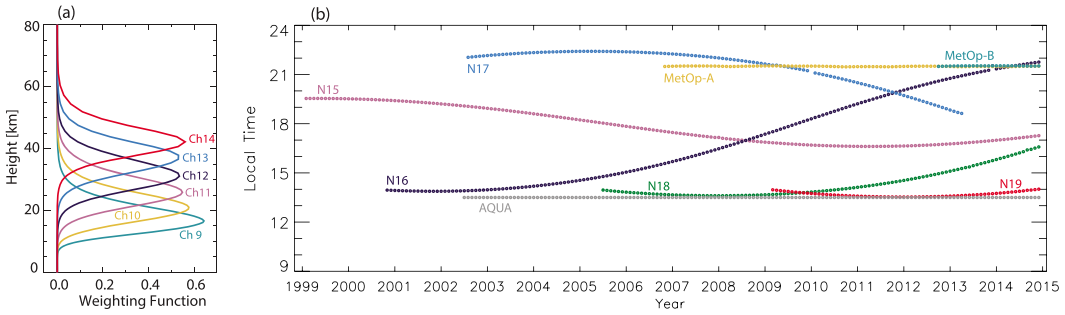

Figure 1. (a) AMSU weighting functions for the upper tropospheric and stratospheric channels (channels 9–14) (from *McLandress et al.* [2015]). (b) Equatorial crossing hour of the ascending node of NOAA platforms (15–19), MetOp-A, and -B, and NASA's AQUA satellite.

EUMETSAT MetOp-A, and NASA AQUA, spanning from 1998 to the present [*Zou and Wang*, 2011; *Zou et al.*, 2013]. The native AMSU-A Level 1b data were intercalibrated using the Integrated Microwave Inter-calibration Approach (IMICA) method to obtain a long-term data product, which permits a better application for climate analysis. This data set includes corrections for the limb effect [*Goldberg et al.*, 2001], which arises because AMSU is a cross-scanning instrument (the atmospheric depth contribution increases away from the near-nadir field of view). Still, we opted to use only information from fields of view 11 to 20 (the least affected by limb effects), covering a swath of ~500 km. Daily orbits (approximately 14 per day) were aggregated to form zonally averaged monthly means for latitude bands covering 90°S–90°N every 30°.

Keckhut et al. [2015] took advantage of the strong orbital drift of NOAA platforms to assess the amplitude of diurnal tides effect on temperature in the middle stratosphere. They showed that tidal correction is a complex task, with the semidiurnal tidal component very difficult to assess and corrections strongly dependent on the tidal model. For climate assessment of temperature trends a satellite's orbital drift represents a constraint, as tidal effects must be removed from stratospheric measurements particularly for channels sampling higher in altitude. We use mainly AMSU data from AQUA (June 2002 to December 2014), as this satellite is kept in a near-constant orbital track, and thus, temperature measurements are not influenced by diurnal-scale tidal effects. AMSU on MetOp platforms also is suitable, except that the first MetOp was operational in late 2006, thus yielding a shorter time series. We examined the consistency of the results obtained by AMSU on AQUA by comparing the series and trends with NOAA 16 for the period 2002–2006 (NOAA 16 orbit drifts after 2004) and with MetOp-A and NOAA 18 for the period (2007–2014).

2.2. SSU and Lidar

In addition to AMSU data, we use SSU and Rayleigh lidar measurements to further analyze our results. Lidar temperature profiles are derived from molecular scattering caused by the emission of a short duration laser pulse in the zenith direction [*Hauchecorne and Chanin*, 1980]. They derive high vertical precision temperature profiles from the low stratosphere up to the mesosphere; however, measurements can only be made in nights with clear sky. Thus, temporal sampling is inhomogeneous. In addition, lidars are geographically scattered and mainly located in the Northern Hemisphere. *Keckhut et al.* [2011] present a thorough description of ground-based lidar temperature series, its attractiveness, and issues involved. Here we use data from three lidar stations located in distinct latitude zones: the Observatoire de Haute Provence (OHP) in southern France (43.91°N, 5.71°E) for the period 1979–2013, the Jet Propulsion Laboratory Table Mountain Facility (TMF) [*McDermid et al.*, 1990] in California (34.41°N, 117.71°W) for 1989–2013, and the Mauna Loa Observatory (MLO) [*McDermid et al.*, 1995] in Hawaii (19.51°N, 155.61°W) for 1993–2013. Data are available through the Network for the Detection of Atmospheric Composition Change (NDACC; http://ndacc-lidar.org/).

For SSU we use the recently released reconstituted and recalibrated data for climate studies by the NOAA STAR [*Zou et al.*, 2014]. Specifically, we use the version 2 gridded (2.5° latitude by 2.5° longitude resolution) pentads data to form monthly means for the period 1979–2006. This multiplatform merged data series takes into account changes in instrument cell pressure and atmospheric carbon dioxide concentration, viewing angle differences, and semidiurnal tides due to orbital drift.

2.3. Linear Trend Estimation

Trends were estimated using multiple regression following *Hauchecorne et al.* [1991]. The multiple regression takes into account the annual, semiannual, terannual, and seasonal cycles (i.e., frequencies of 12, 6, 4, and 3 months, respectively); the quasi-biennial oscillation (QBO) at 10 and 30 hPa; and variations in the solar flux at 10.7 cm. The latter is used as a proxy of the solar short wavelength radiative input. The multiple linear regression is expressed as follows:

$$T(t) = T_0 + \sum_{k=1}^{4}\left[A_k sin\frac{2k\pi}{12}t + B_k sin\frac{2k\pi}{12}t\right] + L(t-\bar{t}) + C\left[\frac{F(t)-\bar{F}}{100}\right] + D_{10}\mathrm{QBO10}(t) + D_{30}\mathrm{QBO30}(t) + T'(t) \quad (1)$$

where t is the time variable, $\bar{t}$ is the mean value of t, T_0 is the constant term, A_k and B_k are the coefficients for the seasonal (periodic) terms, C is the solar flux coefficient, $F(t)$ is the 10.7 cm solar flux at time t, $\bar{F}$ is the mean solar flux during the period of analysis, D_n is the coefficient for the QBO term, with $n = 10$ hPa or $n = 30$ hPa, L is the linear trend component, and $T'(t)$ is the random (residual) component of the temperature. QBO10 and QBO30 are the Singapore monthly mean zonal wind components at 10 and 30 hPa, respectively, obtained from http://www.geo.fu-berlin.de/en/met/ag/strat/produkte/qbo, and the monthly averaged solar flux F at 10.7 cm was obtained from ftp://ftp.geolab.nrcan.gc.ca/data/solar_flux/monthly_averages/maver.txt. The period of 2002–2014 includes a little over one solar cycle, with the descending phase at the beginning, followed by a minimum over ~2007–2009, and a recent ascending phase. We computed the linear correlation between the different proxies and found that they are all very small (between −0.11 and 0.08). Thus, the linear trend is mathematically independent from the solar cycle as the correlation between these two proxies is 0.08.

As in *Hauchecorne et al.* [1991], the confidence interval for each parameter of the fit is calculated based upon the variance of the random component and the correlation between two successive measurements. As such, the uncertainty in the trends is dominated by the variability in the brightness temperatures (and not the uncertainty in the measurement itself). Except for the seasonal trends, all uncertainties presented here represent the 2σ statistical uncertainty level (corresponding to the 95% confidence interval) as in *Hauchecorne et al.* [1991]. Deseasonalized series refer to the total series minus the 12, 6, 4, and 3 month frequency components. Seasonal trends were calculated based on the series of residual plus the linear trend component; a linear fit was then applied on this series considering only the pertinent months for each season. For these trends only we present the 1σ statistical uncertainty levels.

3. Results

3.1. Global and Zonal Mean Averaged Trends

The time series of (near-)global mean and global mean deseasonalized brightness temperatures (BT) for AQUA, NOAA 16 (N16), NOAA 18 (N18), and MetOp-A and are shown in Figure 2. Global average trends estimated from AQUA series (2002–2014) are presented in Table 1 and Figure 3a. Globally, temperatures continued to decline at all levels with values ranging from −0.2±0.3 K/decade for channel 9 to −0.5±0.4 K/decade for channels 12 and 13. These values are slightly smaller than those estimated in previous studies for the preceding decades [e.g., *Ramaswamy et al.*, 2001; *Randel et al.*, 2009].

In order to examine whether these trends can be considered as reliable, we compared trends derived from AQUA with those from N16 for the period of 2002–2006, and N18 and MetOp-A for the common period of 2007–2014 for the three series. AQUA and N16 had close equatorial crossing times until ~2004 and AQUA and N18 until ~2010, after when N16 and N18 started drifting heavily (Figure 1b). The time series of their BT and deseasonalized values are shown in Figure 2. All series have a rather good agreement in the global mean, with very similar mean values (differences ≤0.3 K for most channels; Figure 2a). MetOp-A deseasonalized BT are slightly off compared to AQUA and N18 for the period 2011–2013 (Figure 2b).

Trend estimates are comparable between AQUA and the other platforms for the two distinct periods (Table 2). For the period 2002–2006, temperature tendencies are in good agreement for channels 9–11, but differences are larger in the stratosphere increasing with height. That is due to the larger impact of the N16 orbital drift in the temperature signal, which is more prominent in the stratosphere. Trend estimates for the period 2007–2014, however, show good agreement particularly for the stratospheric channels (12–14) between AQUA and MetOp-A. Trends for this latter period show a consistent cooling in the stratosphere (−1.0 ± 0.7 to −2.1 ± 0.9 K/decade) but warming in the upper troposphere/tropopause region (channel 9).

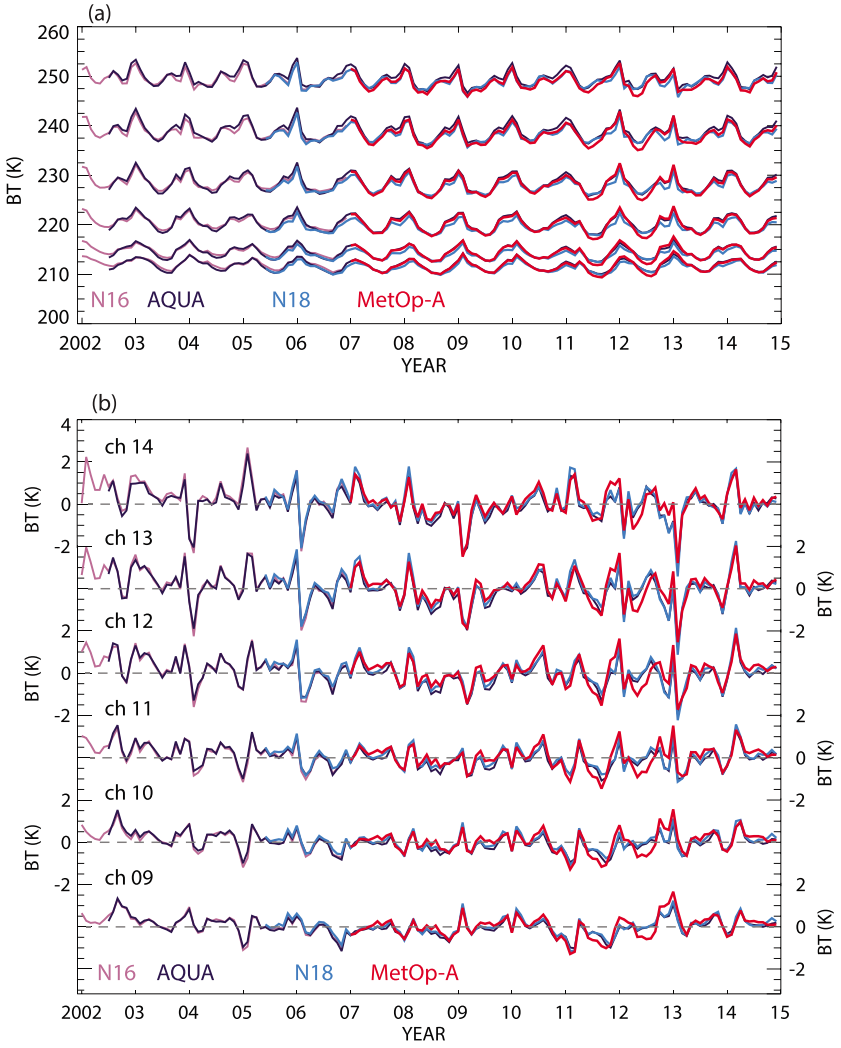

Figure 2. Time series of (a) global mean brightness temperature (BT) and (b) deseasonalized global mean BT (K) issued from AMSU on N16 (purple; only from 2002 to 2006), AQUA (dark blue), N18 (blue), and MetOp-A (red) for channels 9 (bottom) to 14 (top).

The overall agreement between the estimates based on distinct platforms gives us confidence on the robustness of the results based on AMSU on AQUA.

Because the distribution of both dynamical (global stratospheric circulation and tropospheric forcing) and chemical (ozone, water vapor, etc.) forcing is spatially inhomogeneous in the stratosphere, it is instructive also to look at trends at distinct latitudes. For example, the polar stratosphere is dynamically more active than the tropics, and there is also a difference between the austral and boreal polar dynamics. How are these differences reflected in the trends?

Figure 3b and Table 3 show the estimates of linear trends for zonal mean bands of 30° width at low, middle, and high latitudes. In the tropical region (30°S–30°N), channels 9–10 present positive trends ranging from +0.1 ± 0.4 to +0.4 ± 0.4 K/decade, decreasing until −0.7 ± 0.3 K/decade for channel 14. The stratospheric channels in the tropics are the only ones that show significant trends, varying from −0.3 ± 0.3 to −0.7 ± 0.3 K/decade.

Uncertainties are large in the polar regions due to the high wintertime dynamical variability. The northern polar regions present cooling of −0.2 ± 2.6 to −0.5 ± 1.9 K/decade depending on the height, while in the southern polar regions trends range from+0.1 ± 1.2 to −1.1 ± 1.6 K/decade. The southern polar region trend estimate is strongly affected by the September 2002 stratospheric sudden warming [e.g., *Hu and Fu*, 2009]. We recalculated the trends for the period 2003–2014, and we found that trends became very small,

Table 1. Linear Trends (2002–2014) and 2σ Uncertainty (K/Decade) of Globally Averaged AMSU-AQUA Brightness Temperatures for Channels 9–14

Channel	Trend
9	-0.2 ± 0.3
10	-0.3 ± 0.3
11	-0.4 ± 0.3
12	-0.5 ± 0.3
13	-0.5 ± 0.4
14	-0.4 ± 0.4

between 0.1 ± 1.6 and -0.2 ± 1.4 K/decade with little variation in the stratosphere. The uncertainties, however, are still large, and trends are not statistically significant. For the midlatitudes, the observed stratospheric temperature (channels 12–14) trend is negative (i.e., cooling), from -0.1 ± 0.4 to -0.7 ± 0.8 K/decade.

3.2. Seasonal Trends

Besides the latitudinal variability, there exist also seasonal differences, for example, due to the polar vortex breakup in spring and SSWs in winter. Trend estimates were further broken down by season, specifically winter (December, January, February- DJF), spring (March, April, May- MAM), summer (June, July, August- JJA), and autumn (September, October, November- SON) in the Northern Hemisphere and conversely for the Southern Hemisphere. Trend estimates by seasons are presented in Figure 4.

Outside the tropical region, trends present noticeably larger uncertainties in winter and spring than in the summer and autumn, particularly in the northern polar winter (Figure 4a). In northern polar latitudes in autumn and spring (Figures 4b and 4d), channels 11–14 show positive trends. These positive trends are affected by the period chosen, as, for example, trends become negative in autumn when considering the period 2003–2014 but still within the 1σ uncertainty range. In autumn, trend uncertainty is likely related to the occurrence of minor stratospheric warmings, as recently investigated by *Maury et al.* [2016]. The residual plus linear component series of AMSU for this latitude band shows a number of positive temperature anomaly peaks in channels 11–14 in October and November that could be associated with such warmings (not shown).

Between 30°S and 30°N trends are small year round (-1.0 ± 0.3 to 0.6 ± 0.2 K/decade for all channels) but still showing some seasonal variability: trends are smaller and uncertainties are larger in DJF and MAM than in JJA and SON for channels 12–14. In all seasons channel 9 has positive trends (0.1 ± 0.2 to 0.6 ± 0.2 K/decade) except in MAM for Eqt–30°N when the trend is slightly negative but not significant (-0.0 ± 0.2 K/decade). In general, trends tend to be positive for the lowest channels, becoming more negative with height—exception is noted

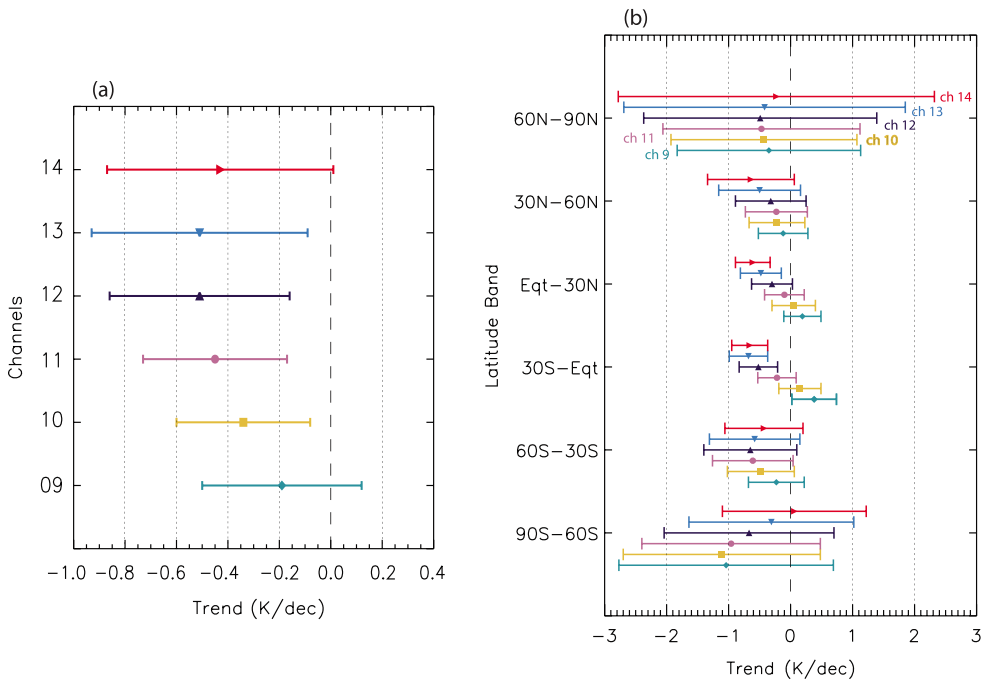

Figure 3. Linear trends (based on AQUA series) for the period 2002–2014, issued from multiparameter regression, of stratospheric temperature for (a) global mean BT and (b) each latitude band shown in the ordinates. Error bars represent the 2σ statistical uncertainty estimates.

Table 2. Linear Trends and 2σ Uncertainty (K/Decade) of AQUA, N16, N18, and MetOp-A Globally Averaged Brightness Temperatures for Channels 9–14[a]

	2002–2006		2007–2014		
Channel	AQUA	N16	AQUA	N18	MetOp-A
9	-1.1 ± 1.2	-1.1 ± 1.2	$+1.3 \pm 0.5$	$+1.4 \pm 0.5$	$+1.8 \pm 0.8$
10	-1.0 ± 1.2	-1.0 ± 1.2	$+0.5 \pm 0.5$	$+0.5 \pm 0.5$	$+0.9 \pm 0.7$
11	-1.0 ± 1.2	-1.2 ± 1.2	-0.2 ± 0.6	-0.4 ± 0.6	$+0.0 \pm 0.8$
12	-1.2 ± 1.4	-1.6 ± 1.5	-1.0 ± 0.7	-1.3 ± 0.8	-1.0 ± 0.9
13	-1.1 ± 1.6	-1.8 ± 1.6	-1.8 ± 0.9	-2.2 ± 0.9	-1.8 ± 1.0
14	-0.6 ± 1.6	-1.4 ± 1.7	-2.1 ± 0.9	-2.6 ± 0.9	-2.3 ± 0.9

[a]Trends are given for the common period of 2002–2006 for AQUA and N16 and for the period 2007–2014 for AQUA, N18, and MetOp-A.

for channels 13 and 14 in summer for the southern tropical region (Eqt–30°S; Figure 4a). The spring and summer trends in the midlatitudes of both hemispheres are small, between -0.9 ± 0.2 and 0.1 ± 0.2 K/decade.

The large spring trend variability in the Southern Hemisphere polar regions (Figure 4d) is linked to the variability of the polar vortex breakup that occurs mostly around September/October [e.g., *Hu and Fu*, 2009; *Garfinkel et al.*, 2013b]. Once more, due to the SSW of September 2002 these trends are strongly affected by the period chosen for trends estimation. We redid the seasonal calculations for the periods 2003–2014 and 2004–2014 to assess the impact of the beginning of series on the estimated trend values. In all seasons, there were no substantial differences in the southern midlatitudes and equatorial regions (not shown). However, in the southern polar regions, a difference of the order of 0.5–1.0 K/decade was observed, which is within the uncertainty range regardless of the period considered.

3.3. Comparisons of AMSU Recent Trends to Long-Term Lidar and SSU Data

Here we seek to use long-term lidar and SSU records to put AMSU-derived results in perspective by comparing recent trends to those of the last few decades at regional scale. Lidar measurements are the only data that spans nearly the entire period of both SSU and AMSU measurements. Lidar and SSU observations for the 1990–2000 decade have shown a seemingly slowing of stratospheric cooling [e.g., *Keckhut et al.*, 2011; *Seidel et al.*, 2016]. We wish to examine whether lidar measurements show a continuous cooling in the long term and also how well do AMSU and lidar measurements compare for the shorter period.

First, we present a brief comparison between AMSU channel 14 (2002–2014), SSU channel 3 (1979–2006), and lidar measurements at OHP (1979–2013), TMF (1989–2013), and MLO (1993–2013). Extensive comparisons between AMSU, SSU, and lidars have been shown elsewhere [*Randel et al.*, 2009; *Keckhut et al.*, 2011; *Funatsu et al.*, 2008, 2011]. AMSU and SSU data were first averaged over an area overpassing each lidar site in order to mitigate spatial sampling differences inherent to lidar and satellite measurements, as was done in *Funatsu et al.* [2008], while lidar data were vertically averaged over the layer 38–42 km, around the peak of AMSU channel 14 weighting function. Despite the amplitude differences among the different measurements and a lower mean temperature of SSU relative to AMSU or lidar (due to differences between AMSU and SSU weighting functions that peak at different altitudes), there is a remarkably good agreement between the time series

Table 3. Linear Trends (2002–2014) and 2σ Uncertainty (K/Decade) of AQUA Zonally Averaged Brightness Temperatures for Channels 9–14

	Latitude Band					
Channel	60°N–90°N	30°N–60°N	Eqt–30°N	Eqt–30°S	30°S–60°S	60°S–90°S
9	-0.4 ± 1.5	-0.1 ± 0.4	$+0.2 \pm 0.3$	$+0.4 \pm 0.4$	-0.2 ± 0.5	-1.0 ± 1.7
10	-0.4 ± 1.5	-0.2 ± 0.5	$+0.1 \pm 0.4$	$+0.2 \pm 0.3$	-0.5 ± 0.5	-1.1 ± 1.6
11	-0.5 ± 1.6	-0.2 ± 0.5	-0.1 ± 0.3	-0.2 ± 0.3	-0.6 ± 0.7	-1.0 ± 1.4
12	-0.5 ± 1.9	-0.3 ± 0.6	-0.3 ± 0.3	-0.5 ± 0.3	-0.7 ± 0.8	-0.7 ± 1.4
13	-0.4 ± 2.3	-0.5 ± 0.7	-0.5 ± 0.3	-0.7 ± 0.3	-0.6 ± 0.7	-0.3 ± 1.3
14	-0.2 ± 2.6	-0.6 ± 0.7	-0.6 ± 0.3	-0.7 ± 0.3	-0.4 ± 0.6	$+0.1 \pm 1.2$

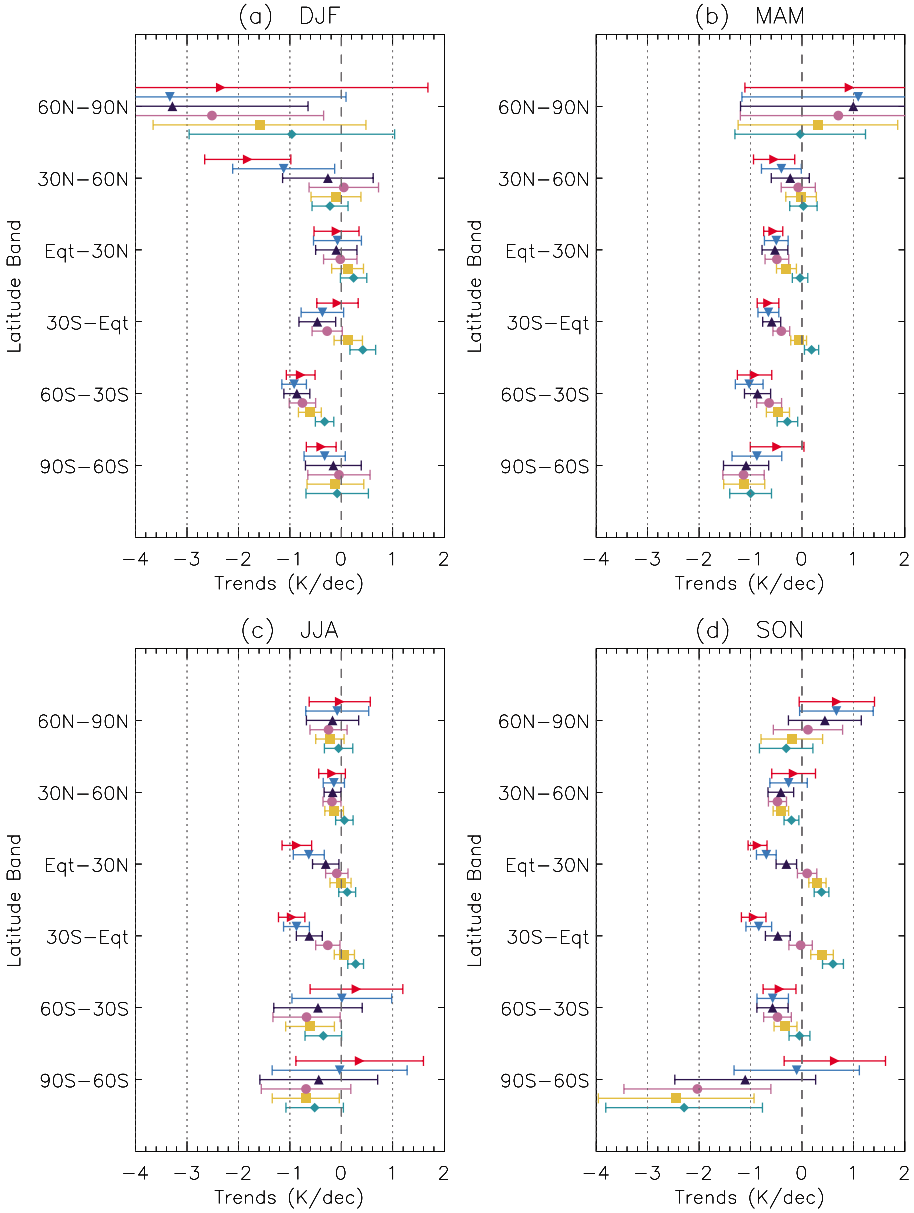

Figure 4. Linear trends of stratospheric temperature for the period 2002–2014 by season: (a) DJF, (b) MAM, (c) JJA, and (d) SON. Error bars represent the 1σ statistical uncertainty. Error bars were cropped (one side only) for Northern Hemisphere polar regions in Figures 4a and 4b in order to keep uniform abscissas for all panels.

(not shown), with a linear correlation r of $r_{OHP,SSU3} = 0.75$ ($r_{OHP,SSU2} = 0.68$), $r_{OHP,AMSU} = 0.63$, and $r_{AMSU,SSU3} = 0.99$ ($r_{AMSU,SSU2} = 0.95$) for the OHP site; $r_{TMF,SSU3} = 0.81$, $r_{TMF,AMSU} = 0.90$, and $r_{AMSU,SSU3} = 0.99$ for the TMF site; and $r_{MLO,SSU3} = 0.80$, $r_{MLO,AMSU} = 0.86$, and $r_{AMSU,SSU3} = 0.97$ for the MLO site. Similar values of correlation between SSU and lidars were found by *Wang and Zou* [2013]. We stress that in this work no joining or merging of SSU and AMSU is attempted, and each series is regarded separately with emphasis on AMSU-based results.

The time series of midstratospheric temperatures anomalies given by lidars, AMSU, and SSU are shown in Figure 5, spanning the period of 1979–2014. These monthly mean anomalies were computed by removing the regressed annual, semiannual, terannual, and seasonal cycles from the full series based on the common period between the three series (July 2002 to May 2006). SSU regional trends (corresponding to the lidar sites) for the period 1979–2006 were estimated to $-0.6 \pm 0.2/-0.9 \pm 0.1/-0.8 \pm 0.1$ K/decade at OHP/TMF/MLO. Trends estimated by the shorter AMSU series (2002–2014) also present cooling in all locations, with values of $-0.8 \pm 1.0/-0.7 \pm 0.6/-0.6 \pm 0.2$ K/decade for OHP/TMF/MLO. These results show that the stratosphere

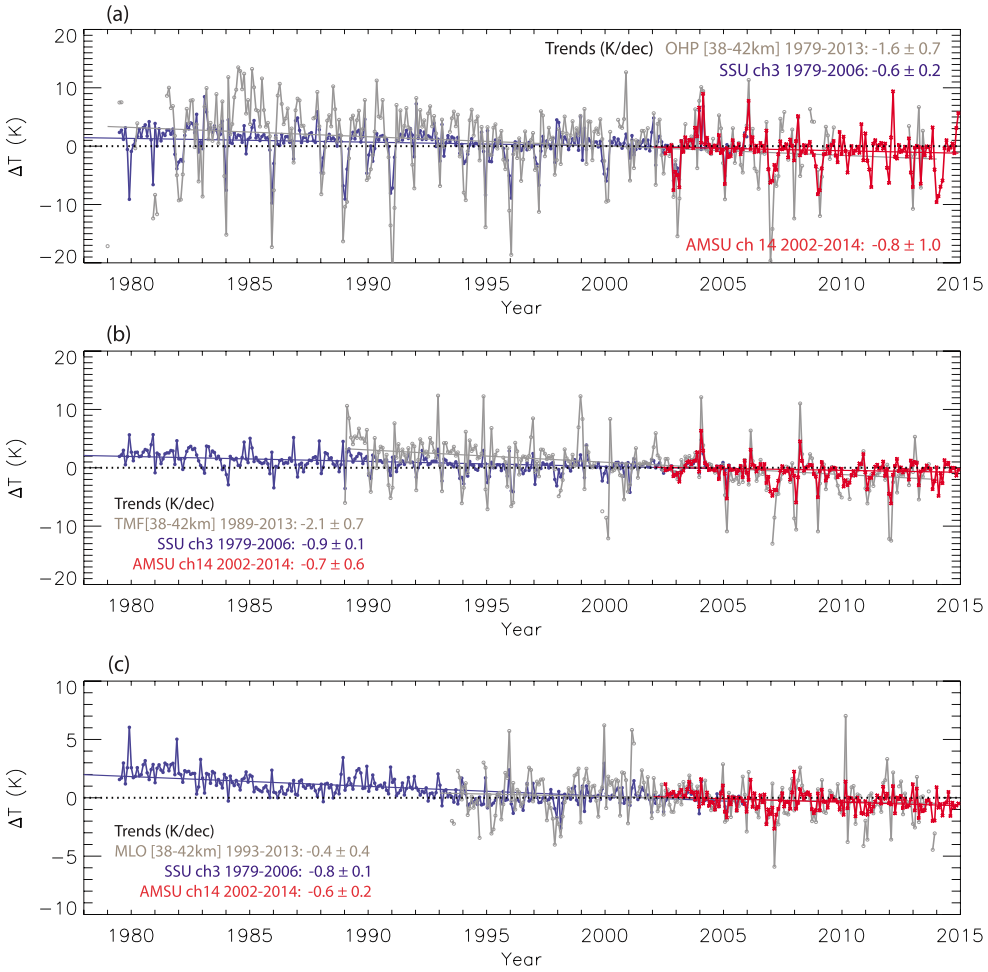

Figure 5. Time series of monthly mean stratospheric temperature anomalies for three lidar sites: (a) OHP (1979–2013), (b) TMF (1989–2013), and (c) MLO (1993–2013). Lidar temperatures (gray) correspond to the 38–42 km layer average and are shown superimposed to SSU channel 3 (blue; 1979–2006) and AMSU channel 14 (red; 2002–2014). Both SSU and AMSU were averaged over the areas (42–47°N, 10°W–20°E) for OHP, (32–37°N, 225–265°E) for TMF, and (17–22°N, 183.5–223.5°E) for MLO. Linear trends and 2σ uncertainty estimates are given in each panel for each instrument.

continued cooling in the recent decade at a rate similar to that of previous decades, and the temperature "flattening" in the 1990s was not sustained. The long-term trend estimated by lidars series is consistently negative, with trend values of $-1.6 \pm 0.7/-2.1 \pm 0.7/-0.4 \pm 0.4$ K/decade for OHP/TMF/MLO. Uncertainties remain large, especially for the OHP site. The OHP site, located in midlatitudes, suffers from a larger influence of the winter polar dynamics [e.g., *Funatsu et al.*, 2011; *Angot et al.*, 2012], which is reflected in the trend uncertainties. The estimates of correlation between OHP and SSU, and the linear trends for this site are in line with those presented by *Wang and Zou* [2013].

The vertical profiles of linear trends estimated using lidar data for the whole archived period and for the recent decade (2002–2013) are shown in Figure 6. Trends are negative and statistically significant at OHP and TMF (Figures 6a and 6b, respectively) for the long term for nearly the entire column from about 30 to 45 km. At OHP, trends range from -0.6 ± 0.5 K/decade at 32 km to -1.6 ± 0.6 K/decade at 44 km, while southwestward at TMF trends range from -1.0 ± 0.4 (at 28 km) to -2.2 ± 0.6 K/decade above 36 km. At MLO, the long-term trend is slightly negative ($> -0.7 \pm 0.4$ K/decade) above 35 km (Figure 6c). Because trends are closer to neutrality at MLO (particularly below 35 km), uncertainties are large relative to the trend itself.

For the most recent decade (2002–2013), except for some altitude ranges at TMF and MLO, trends from lidars are mostly not statistically significant (Figures 6d–6f). Even if not statistically significant, we can still derive some insight as to the local tendencies at these sites. In this period trends are mostly negative varying from

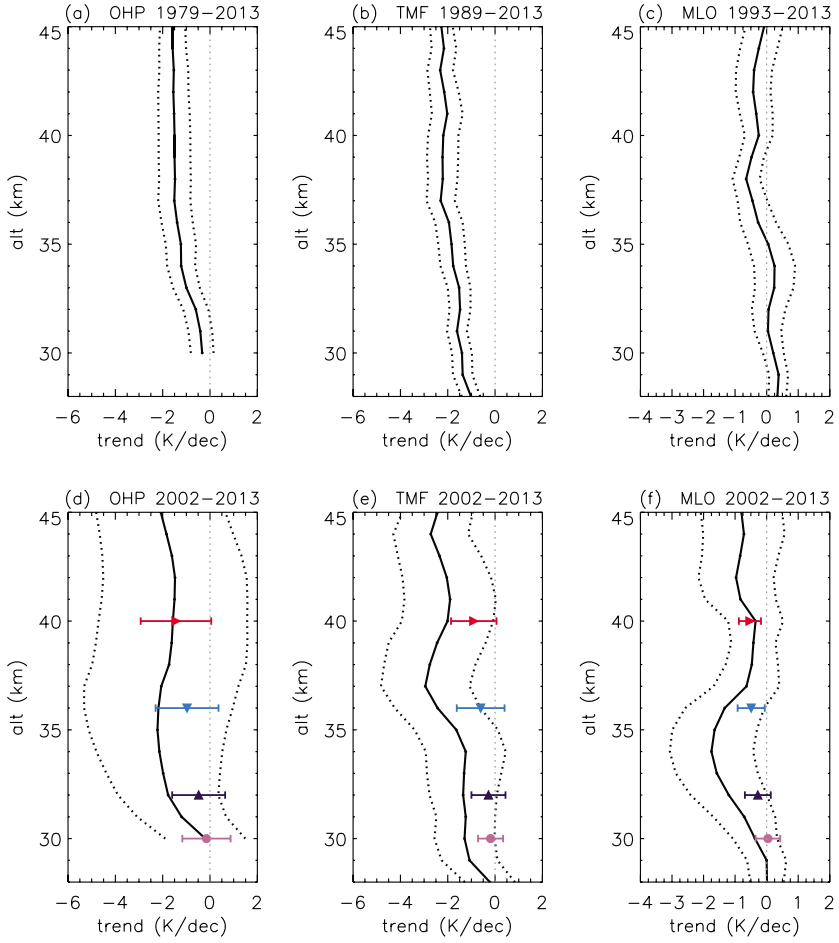

Figure 6. Vertical profiles of linear trends (solid lines) for three lidar sites: (a, d) OHP, (b, e) TMF, and (c, f) MLO, for the total period of data archives (Figures 6a–6c) and for the commom period of the recent decade (2002–2013; Figures 6d–6f). Linear trends derived from AMSU-AQUA were superimposed to the lidar estimates for the recent decade for channels 11–14. Error bars and dashed lines represent the 2σ statistical uncertainty.

-0.2 ± 1.7 to -2.2 ± 2.9 K/decade at OHP, -0.2 ± 1.0 to -3.0 ± 1.9 K/decade at TMF, and $+0.0 \pm 0.6$ to -1.8 ± 1.3 K/decade at MLO (Figures 6d–6f). The AMSU-derived tendencies show that only channels 13 and 14 at MLO present significant trends, both at -0.5 ± 0.4 K/decade. There is overall negative trends for the stratospheric channels (11–14) at the three sites (Figures 6d–6f) as shown in Table 4, but uncertainties are comparable to or larger than the trends themselves. Trend estimates from lidars were found to be generally cooler than AMSU-based estimates. Although AMSU temperatures were averaged over an area overpassing a lidar, trend estimates differences are still present largely due to the irregular temporal sampling by lidars

Table 4. Linear Trends (2002–2013) and 2σ Uncertainty (K/Decade) Based On AQUA Values Averaged Over an Area Encompassing a Lidar Site for Channels 9–14

	Trend		
	OHP	TMF	MLO
Channel	(42–47°N; 10°W–20°E)	(32–37°N; 225–265°E)	(17–22°N; 183.5–223.5°E)
9	$+0.2 \pm 0.8$	-0.2 ± 0.5	$+0.7 \pm 0.5$
10	$+0.0 \pm 0.9$	-0.3 ± 0.6	$+0.3 \pm 0.5$
11	-0.2 ± 1.0	-0.2 ± 0.5	$+0.0 \pm 0.4$
12	-0.5 ± 1.1	-0.3 ± 0.7	-0.3 ± 0.4
13	-1.0 ± 1.3	-0.6 ± 1.0	-0.5 ± 0.4
14	-1.4 ± 1.5	-0.9 ± 1.0	-0.5 ± 0.4

(which can make measurements only in nights with clear sky) compared to a mostly regular temporal sampling by satellites, as demonstrated by *Funatsu et al.* [2008].

4. Summary and Discussion

We used AQUA AMSU-IMICA channels 9–14 (upper troposphere to middle stratosphere) data to assess global, zonal, and seasonal trends for the period 2002–2014. Global averaged temperature trend estimates show that the stratosphere continues to cool at a global rate of approximately -0.4 ± 0.3 to -0.5 ± 0.4 K/decade for channels above ~25 km (channels 11 and up). Latitudinal bands show a large range of temperature trends, depending on the channel and on the zonal band. Outside the polar regions, trends vary between -0.7 ± 0.3 and 0.4 ± 0.4 K/decade. In general, polar regions show stronger trends but large uncertainties (due to the high dynamical variability), with values ranging from -1.1 ± 1.7 to $+0.1 \pm 1.2$ K/decade for the southern polar region and between -0.2 ± 2.6 and -0.5 ± 1.9 K/decade in the northern high latitudes. Finally, regarding trends seasonality, within the tropical region seasonal variation (except in DJF) of stratospheric cooling is observed for channels 12 and above, with cooling typically stronger with height. The southern midlatitude region (30°–60°S) also present consistently negative cooling in the stratosphere (above ~25km) from spring to autumn, with values varying from -1.0 ± 0.6 up to -0.4 ± 0.6 K/decade.

We also calculated trends based on regional AMSU temperature averages over three lidar sites located in the midlatitudes (OHP), subtropics (TMF), and tropics (MLO). Trends within the tropics are positive for channels 9 and 10 ($+0.7 \pm 0.5$ and $+0.3 \pm 0.5$ K/decade, respectively, for the period 2002–2013) and negative for the stratospheric channels (12–14) in all sites (Table 4). Consistently, trends calculated based on lidar data for the period 2002–2013 (the latest year available in the NDACC database) show cooling throughout the stratospheric layer. Previous studies have pointed to a flattening of stratospheric temperature trends between the mid-1990s to the mid-2000s [e.g., *Keckhut et al.*, 2011; *Seidel et al.*, 2016], noticeable, for example, in Figure 5 by the three lidars. The most recent AMSU and lidar data indicate, however, that this (apparent) plateau was not sustained, and stratospheric temperatures continue to decrease.

The latest WMO ozone assessment [*Pawson et al.*, 2014] showed that observations and models exhibit a slight near-global (60°N–60°S) ozone trend reversal in the middle stratosphere at around 42 km (corresponding approximately to AMSU channel 14) starting at the end of the 1990s. The increase in ozone is most visible in the midlatitudes (35°–60° latitude bands in both hemispheres) but small in the tropical region.

In the tropical region, *Nedoluha et al.* [2015] have shown that there was a significant decrease in O_3 near ~10 hPa (close to channel 12) based on measurements of the NASA Aura Microwave Limb Sounder (MLS) for the period 2004–2013. They explain that ozone concentration in this region is very sensitive to variations in NO_y and that the observed O_3 decrease can be interpreted as a spatially localized, long-term increase in NO_y. Decrease in NO_y, in turn, is linked to changes in dynamics, for example, decreased upwelling in the tropics, leading to a larger production of NO_y and subsequent destruction of O_3. The decrease in O_3 in the tropics could partially explain the seemingly strengthening in the cooling trends in the recent past (compared to the long-term trends) observed at MLO (Figures 6c and 6f). On the other hand, chemistry climate simulations using the GEOSCCM model showed that no trends were observed in the lower stratosphere tropical temperature anomalies but a cooling trend above 30 km (channels 12–14) caused mainly by greenhouse gases (V. Aquila, personal communication, 2015). In general, *Aquila et al.* [2016] have shown that in global scale after 2000, GHG are the main contributors for cooling above 20 km, but the rate of cooling is hampered by the decrease in ODS and with an important contribution from the ascending phase of the solar cycle.

Finally, the correlation coefficients between predictors (linear term, QBO, and solar flux) were found to be small, indicating that they are mathematically independent. The regression coefficients for the solar cycle (not shown) displayed positive and statistically significant values for channel 14 in the tropical region, mostly positive and significant in the southern midlatitudes (all channels) and southern polar regions (channels 9–11). The shape of the latitudinal distribution of regression coefficients showed a somewhat qualitatively similar distribution of that found by *Randel et al.* [2016] based on more than three decades of combined SSU, SABER, and MLS, as they found large values for MSU4 (close to channel 9) in the Southern Hemisphere polar regions and coefficient values increasing with SSU channel within the tropics. In our study, QBO regression coefficients were found to be mostly significant in the tropical region, with values changing with height following the phase shift between the winds at 10 and 30 hPa. This feature was found to be particularly prominent in the equatorial region (15°S–15°S) as shown in Figure 7. The correlation with QBO at 30 hPa peaks in channel

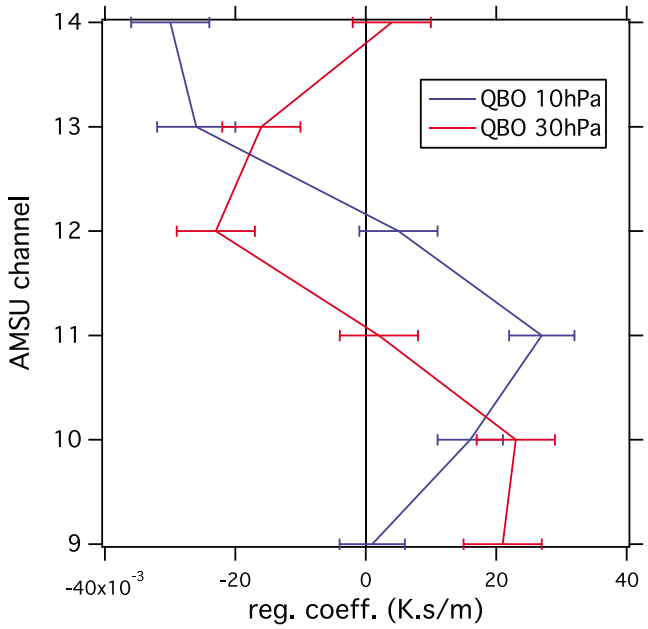

Figure 7. Vertical profiles of regression coefficients (K.s/m) for the QBO predictors at 10 hPa (blue) and 30 hPa (red) in the equatorial region (15°S–15°N). Error bars represent the 2σ statistical uncertainty.

10 (around 50 hPa) and in channel 11 (around 25 hPa) with QBO at 10 hPa. This is in agreement with *Baldwin et al.* [2001], which showed that the equatorial temperature is correlated with the vertical gradient of zonal wind that peaks lower than the zonal wind itself.

In the present work we did not consider the effect of volcanic aerosols on the trends. The last major volcanic eruption was the Pinatubo in 1991, which injected large amounts of aerosol in the stratosphere and caused tropospheric cooling and increase in stratospheric ozone depletion [e.g., *McCormick et al.*, 1995]. The stratospheric aerosol levels decreased to its "background levels" between 1998 and 2002 [*Mehta et al.*, 2015, and references therein]. Since 2002, a series of minor volcanic eruptions in 2002, 2005, 2006, 2010, and 2011 in the tropics, and also in the northern midlatitudes in 2008 and 2009, have injected aerosols into the stratosphere (up to 25 km) and transported to the adjacent latitudes [*Mehta et al.*, 2015]. These sequence of eruptions led to the increase of stratospheric optical depth (AOD), which in turn have been linked to decrease in global tropospheric temperature over the period 2000–2010 [e.g., *Solomon et al.*, 2011]. *Mehta et al.* [2015] found limited response of the upper troposphere and lower stratosphere temperature, with warming of 0.5–0.8 K for 7 months only in the 16–18.5 km layer after two tropical eruptions. The effect of the AOD increase in the stratospheric temperature trend, however, is difficult to assess as their effects are nonlinear in time and space and would not be adequately assessed with the multiple linear regression method alone used here [*Santer et al.*, 2015].

AMSU observations are at present the only observations of this part of the atmosphere that cover a long period of time in global scale and will continue in the future. They appear as essential for detecting climate change and provide robust measurements for comparisons with climate model outputs.

Acknowledgments
The AMSU-A Climate Data Record (CDR) used in this study was acquired from NOAA's National Climatic Data Center (http://www.ncdc.noaa.gov) with the support of Climserv-IPSL. This CDR was originally developed by Cheng-Zhi Zou and colleagues at NOAA through support from NOAA's CDR Program. The lidar data used in this publication were obtained through the Network for the Detection of Atmospheric Composition Change (NDACC) and are publicly available (see http://www.ndacc.org). This work was supported by the French National Research Agency (ANR) through the StraDyVariUS project (ANR-13-BS06-0011), by the EU H2020 project ARISE2 (Atmospheric dynamics Research InfraStructure in Europe), and is a contribution to the WCRP/SPARC Temperature Trends Group. We are grateful for the critical comments from three anonymous Reviewers that helped improve the manuscript.

References

Angot, G., P. Keckhut, A. Hauchecorne, and C. Claud (2012), Contribution of stratospheric warmings to temperature trends in the middle atmosphere from the lidar series obtained at Haute-Provence Observatory (44°N), *J. Geophys. Res.*, *117*, D21102, doi:10.1029/2012JD017631.

Aquila, V., W. H. Swartz, P. R. Colarco, S. Pawson, L. M. Polvani, R. S. Stolarski, and D. W. Waugh (2016), Isolating the roles of different forcing agents in global stratospheric temperature changes using model integrations with incrementally added single forcings, *J. Geophys. Res. Atmos.*, *121*, doi:10.1002/2015JD023841.

Austin, J., et al. (2009), Coupled chemistry climate model simulations of stratospheric temperatures and their trends for the recent past, *Geophys. Res. Lett.*, *36*, L13809, doi:10.1029/2009GL038462.

Baldwin, M. P., et al. (2001), The quasi-biennial oscillation, *Rev. Geophys.*, *39*, 179–229.

Cagnazzo, C., C. Claud, and S. Hare (2006), Aspects of stratospheric longterm changes induced by ozone depletion, *Clim. Dyn.*, *27*, 101–111, doi:10.1007/s00382-006-0120-1.

Funatsu, B. M., C. Claud, P. Keckhut, and A. Hauchecorne (2008), Cross-validation of Advanced Microwave Sounding Unit and lidar for long-term upper-stratospheric temperature monitoring, *J. Geophys. Res.*, *113*, D23108, doi:10.1029/2008JD010743.
Funatsu, B. M., C. Claud, P. Keckhut, W. Steinbrecht, and A. Hauchecorne (2011), Investigations of stratospheric temperature regional variability with lidar and Advanced Microwave Sounding Unit, *J. Geophys. Res.*, *116*, D08106, doi:10.1029/2010JD014974.
Garfinkel, C. I., L. D. Oman, E. A. Barnes, D. W. Waugh, M. H. Hurwitz, and A. M. Molod (2013a), Connections between the spring breakup of the Southern Hemisphere polar vortex, stationary waves, and air-sea roughness, *J. Atmos. Sci.*, *70*, 2137–2151, doi:10.1175/JAS-D-12-0242.1.
Garfinkel, C. I., D. W. Waugh, L. D. Oman, L. Wang, and M. M. Hurwitz (2013b), Temperature trends in the tropical upper troposphere and lower stratosphere: Connections with sea surface temperatures and implications for water vapor and ozone, *J. Geophys. Res. Atmos.*, *118*, 9658–9672, doi:10.1002/jgrd.50772.
Gillet, N. P., et al. (2012), Attribution of observed changes in stratospheric ozone and temperature, *Atmos. Chem. Phys.*, *11*, 599–609, doi:10.5194/acp-11-599-2011.
Goldberg, M. D., D. S. Crosby, and L. Whou (2001), The limb adjustment of AMSU-A observations: Methodology and validation, *J. Appl. Meteorol.*, *40*, 70–83.
Hansen, J., et al. (1997), Forcings and chaos in interannual to decadal climate change, *J. Geophys. Res.*, *102*, 25,679–25,720.
Hauchecorne, A., and M.-L. Chanin (1980), Density and temperature profiles obtained by lidar between 35 and 70 km, *Geophys. Res. Lett.*, *7*, 565–568.
Hauchecorne, A., M.-L. Chanin, and P. Keckhut (1991), Climatology and trends of the middle atmospheric temperature (33–87 km) as seen by Rayleigh lidar over the south of France, *J. Geophys. Res.*, *96*(D8), 15,297–15,309, doi:10.1029/91JD01213.
Hu, Y., and Q. Fu (2009), Stratospheric warming in Southern Hemisphere high latitudes since 1979, *Atmos. Chem. Phys.*, *9*, 4329–4340.
Keckhut, P., et al. (2011), An evaluation of uncertainties in monitoring middle atmosphere temperatures with the ground-based lidar network in support of space observations, *J. Atmos. Sol. Terr. Phys.*, *73*, 627–642, doi:10.1016/j.jastp.2011.01.003.
Keckhut, P., B. M. Funatsu, C. Claud, and A. Hauchecorne (2015), Tidal effects on stratospheric temperature series derived from successive advanced microwave sounding units, *Q. J. R. Meteorol. Soc.*, *141*, 477–483, doi:10.1002/qj.2368.
Maury, P., C. Claud, E. Manzini, A. Hauchecorne, and P. Keckhut (2016), Characteristics of stratospheric warming events during Northern winter, *J. Geophys. Res. Atmos.*, *121*, 5368–5380, doi:10.1002/2015JD024226.
McCormick, M. P., L. W. Thomason, and C. R. Trepte (1995), Atmospheric effects of the Mt Pinatubo eruption, *Nature*, *373*, 399–404, doi:10.1038/373399a0.
McDermid, I. S., S. M. Godin, and L. O. Lindqvist (1990), Ground-based laser dial system for long-term measurements of stratospheric ozone, *Appl. Opt.*, *29*, 3603–3612.
McDermid, I. S., T. D. Walsh, A. Deslis, and M. L. White (1995), Optical-systems design for a stratospheric lidar system, *Appl. Opt.*, *34*, 6201–6210.
McLandress, C., T. S. Shepherd, A. I. Jonsson, T. von Clarmann, and B. Funke (2015), A method for merging nadir-sounding climate records, with an application to the global-mean stratospheric temperature data sets from SSU and AMSU, *Atmos. Chem. Phys.*, *15*, 9271–9284, doi:10.5194/acp-15-9271-2015.
Mehta, S. K., M. Fujiwara, T. Tsuda, and J.-P. Vernier (2015), Effect of recent minor volcanic eruptions on temperatures in the upper troposphere and lower stratosphere, *J. Atmos. Sol. Terr. Phys.*, *129*, 99–110, doi:10.1016/j.jastp.2015.04.009.
Nash, J., and R. Saunders (2015), A review of stratospheric sounding unit radiance observations for climate trends and reanalyses, *Q. J. R. Meteorol. Soc.*, *141*, 2103–2113, doi:10.1002/qj.2505.
Nedoluha, G. E., D. E. Siskind, A. Lambert, and C. Boone (2015), The decrease in mid-stratospheric tropical ozone since 1991, *Atmos. Chem. Phys.*, *15*, 4215–4224, doi:10.5194/acp-15-4215-2015.
Pawson, S., W. Steinbrecht, A. J. Charlton-Perez, M. Fujiwara, A. Y. Karpechko, I. Petropavlovskikh, J. Urban, and M. Weber (2014), Update on global ozone: Past, present, and future, in *Scientific Assessment of Ozone Depletion, Global Ozone Res. and Monit. Project - Rep. 55*, edited by A.-L. Ajavon et al., World Meteorol. Organ., Geneva, Switzerland.
Randel, W. J., et al. (2009), An update of observed stratospheric temperature trends, *J. Geophys. Res.*, *114*, D02107, doi:10.1029/2008JD010421.
Randel, W. J., A. K. Smith, F. Wu, C.-Z. Zhou, and H. Qian (2016), Stratospheric temperature trends over 1979–2015 derived from combined SSU, MLS, and SABER satellite observations, *J. Clim.*, *29*, 4843–4859, doi:10.1175/JCLI-D-15-0629.1.
Ramaswamy, V., et al. (2001), Stratospheric temperature trends: Observations and model simulations, *Rev. Geophys.*, *39*, 71–122.
Santer, B. D., et al. (2015), Observed multivariable signals of late 20th and early 21st century volcanic activity, *Geophys. Res. Lett.*, *42*, 500–509, doi:10.1002/2014GL062366.
Seidel, D. J., J. Li, C. Mears, I. Moradi, J. Nash, W. J. Randel, R. Saunders, D. W. J. Thompson, and C.-Z. Zou (2016), Stratospheric temperature changes during the satellite era, *J. Geophys. Res. Atmos.*, *121*, 664–681, doi:10.1002/2015JD024039.
Shine, K. P., et al. (2003), A comparison of model-simulated trends in stratospheric temperatures, *Q. J. R. Meteorol. Soc.*, *129*, 1565–1588, doi:10.1256/qj.02.186.
Solomon, S., J. S. Daniel, R. R. Neely III, J.-P. Vernier, E. G. Dutton, and L. W. Thomason (2011), The persistently variable "background" stratospheric aerosol layer and global climate change, *Science*, *333*, 866–870, doi:10.1126/science.1206027.
Son, S.-W., N. F. Tandon, L. M. Polvani, and D. W. Waugh (2009), Ozone hole and Southern Hemisphere climate change, *Geophys. Res. Lett.*, *36*, L15705, doi:10.1029/2009GL038671.
Thompson, D. W. J., D. J. Seidel, W. J. Randel, C.-Z. Zou, A. H. Butler, C. Mears, A. Osso, C. Long, and R. Lin (2012), The mystery of recent stratospheric temperature trends, *Nature*, *491*, 692–697, doi:10.1038/nature11579.
Wang, L., and C.-Z. Zou (2013), Intercomparison of SSU temperature data records with Lidar, GPS RO, and MLS observations, *J. Geophys. Res. Atmos.*, *118*, 1747–1759, doi:10.1002/jgrd.50162.
Wang, L., C.-Z. Zou, and H. Qian (2012), Construction of stratospheric temperature data records from stratospheric sounding units, *J. Clim.*, *25*, 2931–2946.
Waugh, D. W., W. J. Randel, S. Pawson, P. A. Newman, and E. R. Nash (1999), Persistence of the lower stratospheric polar vortices, *J. Geophys. Res.*, *104*, 27,191–27,201, doi:10.1029/1999JD900795.
World Meteorological Organization (2014), Scientific Assessment of Ozone Depletion: 2014, *Global Ozone Res. and Monit. Project – Rep. No. 55*, 416 pp., Geneva, Switzerland.
Young, P. J., A. H. Butler, N. Calvo, L. Haimberger, P. J. Kushner, D. R. Marsh, W. J. Randel, and K. H. Rosenlof (2013), Agreement in late twentieth century Southern Hemisphere stratospheric temperature trends in observations and CCMVal-2, CMIP3, and CMIP5 models, *J. Geophys. Res. Atmos.*, *118*, 605–613, doi:10.1002/jgrd.50126.

Zou, C.-Z., and W. H. Wang (2011), Intersatellite calibration of AMSU-A observations for weather and climate applications, *J. Geophys. Res*, *116*, D23113, doi:10.1029/2011JD016205.

Zou, C.-Z., W. Wang, and NOAA CDR Program (2013), NOAA Fundamental Climate Data Record (FCDR) of AMSU-A Level 1c Brightness Temperature, Version 1.0. [data subset: All data from 2002–2014],NOAA National Climatic Data Center, doi:10.7289/V5X63JT2, [access date: 26/12/2015].

Zou, C.-Z., H. Qian, W. Wang, L. Wang, and C. Long (2014), Recalibration and merging of SSU observations for stratospheric temperature trend studies, *J. Geophys. Res. Atmos.*, *119*, 13,180–13,205, doi:10.1002/2014JD021603.